HYDROELASTIC OF AXISYMMETRIC SYSTEMS BY A FINITE ELEMENT METHOD

R. J. Guyan,* B. H. Ujihara* and P. W. Welch*

North American Rockwell Corporation

The irrotational motion of incompressible fluids may be completely described by proper specification of velocities at and normal to the fluid boundaries. This statement, expressed in integral form, is known as the Neumann problem. A finite element solution of this integral equation is obtained for flow within axisymmetric bodies following the method of Smith and Pierce. This solution results in a description of the fluid mass properties consistent with that of the elastic container boundary. The combination of these fluid and container properties by the direct stiffness method leads to a straightforward formulation of the eigenproblem describing hydroelastic motion of liquid propellants in a shell container. Shell description is in terms of the conical frustum element by Grafton and Strome. Free surface effects are found to be accountable by idealizing the surface as concentric annular elements restrained by a concentrated axial stiffness. Isentropic ullage pressure/volume relationship is used to describe the influence of ullage volume changes on the natural vibration. Condition of liquid volume constancy imposed by incompressibility is incorporated as a generalized constraint condition in the manner described by Greene. Computer results show fair agreement with data in the literature.

*Members of the Technical Staff, Structures & Dynamics, Structures Design, Space Division

NOMENCLATURE

$\mathbf{A}$	velocity influence coefficients
$\mathbf{B}$	velocity potential influence coefficients
$\mathbf{C}$	flexibility matrix
$\mathbf{D}$	dynamical matrix
$E(k)$, $K(k)$	complete elliptic integrals of the first and second kind
$\mathbf{F}$	generalized forces
$\mathbf{I}$	identity matrix
$\mathbf{K}_c$	container stiffness matrix
$\mathbf{K}_p$	ullage pressure stiffness matrix
$\mathbf{K}_s$	liquid free surface stiffness matrix
$\mathbf{M}$	mass matrix
$\mathbf{S}$	banded integrating matrix
T	kinetic energy
ΔV_ℓ	total liquid volume change
$\Delta \mathbf{V}_u$	volumetric changes
V_o	static ullage volume
$\mathbf{X}$	matrix of coefficients relating velocities in the x-direction to the source strengths
$\mathbf{Y}$	matrix of coefficients relating velocities in the y-direction to the source strengths
g	gravitational acceleration
k	modulus of elliptic integrals
p	pressure at a point
p_o	static ullage pressure
r	distance between two points p and q, r(p,q)
s	coordinate measuring arc length

NOMENCLATURE (CONT)

t, n	container nodal circle tangential and normal displacements
u, w	container nodal circle axial and radial displacements
$\mathbf{u}$	generalized displacements
u_n	normal displacements
u_o	eigenvectors
u_s	liquid free surface displacements
v_n	normal velocities
x, y	cartesian coordinates
Φ	velocity potential
Ω	body force
α	angle between axis of revolution (x) and local tangent line
β	container nodal circle rotation
γ	gas constant
σ	source strengths
ρ	liquid density
ξ, η	coordinates of particular points

Subscripts

u, w, β, t, n	refer to displacements defined above
$c\ell$	refer to container nodal circles in contact with liquid
cg	refer to container nodal circles in contact with ullage gas
s	refer to liquid free surface elements

Matrix Notation

$[\ ]$	square or rectangular matrices
$\{\ \}$	column matrix

Matrix Superscript

T	transpose of a matrix

SECTION I

INTRODUCTION

Applicability of finite element methods to solution of problems in continuum mechanics is rapidly being exploited. For example, Zienkiewicz and Cheung (Reference 1) in their recently published book discuss several such applications in the analysis of heat conduction, fluid flow, and the vibration of submerged structures. The paper presented here is concerned with the hydroelasticity of liquid propellant contained in an axisymmetric elastic shell.

For those associated with aerospace structural dynamics, this particular phenomenon of longitudinal slosh coupled with elastic deformations of the container wall is mostly familiar for its important role in the notorious Pogo problem. Because of the importance of this hydroelastic problem, numerous approaches to its solution have been taken during the past few years. The majority of these appear to have been based upon classical techniques, but a few have employed finite element methods.

Of these, two have come to the attention of the authors. The first is that presented by Palmer and Asher (Reference 2). In that approach the displacement method was employed for the overall structural analysis, but the fluid effects were described in terms of series expansion of the velocity potential. Their results for the fundamental structural mode of a model cylinder-bulkhead configuration agreed reasonably well with their test data. In a more recent formulation, Tong (Reference 3) described the fluid mass in terms of the velocity potentials of finite toroidal elements. This mass system was then combined with the structural system employing the displacement method. Actual numerical results employing this formulation, however, were not obtained. It may be added that this method of describing the fluid mass is conceptually consistent with the finite element technique. The approach described by Zienkiewicz and Cheung (Reference 1) also discretizes the fluid region into finite elements.

In the finite element method presented here, a still different approach is utilized for the derivation of the fluid mass matrix. Basically it utilizes a technique first developed by Smith and Pierce (Reference 4) more than ten years ago for the calculation of steady potential flow about axisymmetric bodies of arbitrary shape. In this approach a discretization of the fluid region itself is not necessary. Only the boundary already described in the structural idealization is required. In this context, it must be noted that the quiescent liquid free surface

under steady gravitational acceleration along the axis is treated simply as part of the structural boundary. Aesthetically, the fact that finite elements are employed only for the boundary of the fluid region does depart from the basic philosophy underlying the finite element technique. However, the comparative advantages and disadvantages of this method of generating the fluid mass matrix remain to be established.

SECTION II

PROBLEM DEFINITION AND MODEL DESCRIPTION

The problem considered is the calculation of the axisymmetric vibration behavior of the elastic container-liquid system shown in Figure 1. The container is represented by conical frustum elements with circular plates providing closure at each end. Similar frusta idealize the container support. An inviscid, incompressible liquid partially fills the container while a massless pressurant gas is enclosed in the remaining volume. The liquid free surface is comprised of concentric annular rings which may be regarded as structural elements restrained in the normal direction by concentrated springs. In addition the mean free surface displacement is governed by the condition of constancy in total volume.

While container nodal circles initially possess axial, radial and rotational degrees of freedom, only normal displacements at circles in contact with liquid are finally retained. Axial displacements of the free surface elements complete the degrees of freedom included in the model. Mass of the container is neglected in comparison with the liquid mass.

The condition of zero normal flow across the fluid boundary is satisfied by a system of finite source elements whose geometric properties are coincident with those employed for the matching structural elements.

All displacements are small within the restriction of linear dynamical systems and motion is simple harmonic.

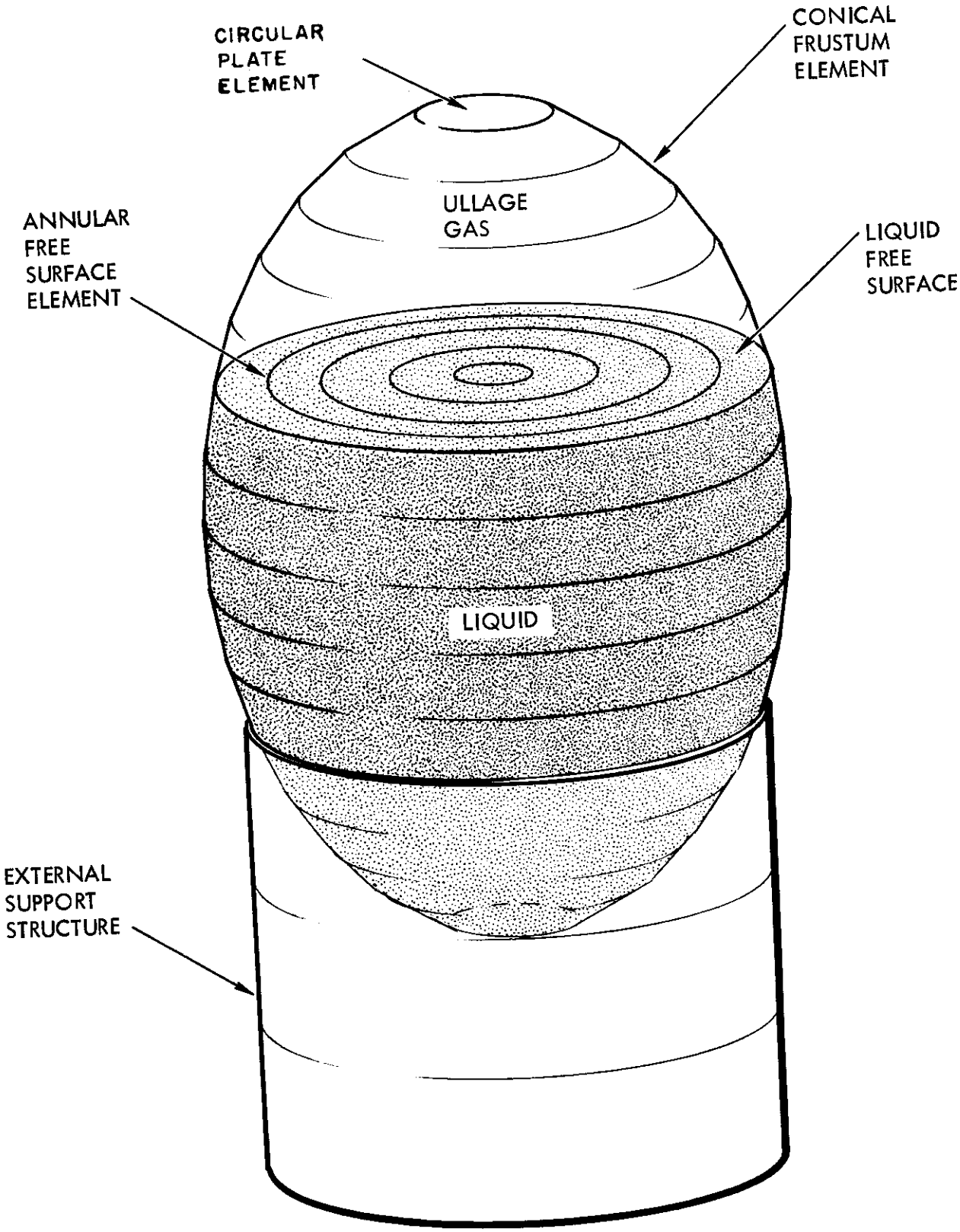

Figure 1. Elastic Container-Liquid Model

SECTION III

FORMULATION OF THE EIGENVALUE PROBLEM

The basic equations of the hydroelastic problem are introduced here, and the free vibration eigenproblem formulated. Full development of the matrices involved is included in the following sections.

Normal displacements of the elastic container and liquid free surface are expressed in terms of the applied pressure forces by the flexibility equations

$$\{u_n\} = [C]\{F\} \tag{1}$$

Hydrodynamic influence coefficients relating normal velocities at nodal circles to source element strengths along the boundary can be written in matrix form as

$$\{v_n\} = [A]\{\sigma\} \tag{2}$$

The velocity potential at nodal circles can be similarly expressed.

$$\{\Phi\} = [B]\{\sigma\} \tag{3}$$

The pressure equation for this problem is

$$\left\{\frac{p}{\rho}\right\} = \left\{\frac{\partial \Phi}{\partial t}\right\} - \{\Omega\} - \frac{1}{2}\left\{(\nabla\Phi \cdot \nabla\Phi)\right\} \tag{4}$$

Ω represents the body force. In a time constant gravitational potential the body force associated with the mean fluid depth must also be time independent. For the eigenproblem formulation, then, the body force associated with the mean fluid depth may safely be removed from the pressure equation. The remaining effect of gravitational inertia forces on the free surface oscillation is treated in a later section as a structural parameter. Neglecting squared velocity terms, and integrating to obtain total pressure forces, the pressure equation becomes

$$\{F\} = \rho [S] \left\{\frac{\partial \Phi}{\partial t}\right\} \tag{5}$$

where $[S]$ is a banded integrating matrix. The first three matrix equations, together with the linearized Bernoulli equation, are sufficient to formulate the eigenproblem for a hydroelastic system.

For simple harmonic motions, normal displacements are written

$$\{u_n\} = \{u_o\} \sin \omega t \tag{6}$$

Normal velocities are then given by

$$\left\{\frac{d\,u_n}{dt}\right\} = \left\{v_n\right\} = \left\{u_o\right\}\omega\,\cos\omega t \tag{7}$$

Eliminating source strengths between Equations 2 and 3 results in

$$\left\{\Phi\right\} = \left[B\right]\left[A\right]^{-1}\left\{u_o\right\}\omega\,\cos\omega t \tag{8}$$

Differentiating this equation and introducing Equations 1 and 5 gives

$$\left\{\frac{\partial\Phi}{\partial t}\right\} = -\left[B\right]\left[A\right]^{-1}\left\{u_o\right\}\omega^2\,\sin\omega t = \frac{1}{\rho}\left[S\right]^{-1}\left[C\right]^{-1}\left\{u_o\right\}\sin\omega t \tag{9}$$

or

$$\left[C\right]\left[S\right]\left[B\right]\left[A\right]^{-1}\left\{u_o\right\} = -\frac{1}{\rho\omega^2}\left\{u_o\right\} \tag{10}$$

in standard eigenproblem form.

The dynamical matrix is

$$\left[D\right] = \left[C\right]\left[S\right]\left[B\right]\left[A\right]^{-1} \tag{11}$$

with eigenvalues

$$\lambda = -\frac{1}{\rho\omega^2} \tag{12}$$

SECTION IV

DERIVATION OF THE STIFFNESS MATRIX

Generation of the system stiffness matrix is by the direct stiffness method. Container stiffness, stiffness of the liquid free surface, the effects of ullage pressure, and liquid incompressibility are included as integral parts of the derivation. The condition of liquid incompressibility also applies to the system mass matrix.

ELASTIC CONTAINER

The elastic properties of the container are described by the conical frustum stiffness matrix due to Grafton and Strome (Reference 5). Displacements parallel and perpendicular to the axis of revolution and rotation are included at each nodal circle. Circular plate elements are used to close out the container on the axis of revolution. The plate stiffness equation is given in Appendix I. After assembly of the container element stiffness matrices, force free degrees of freedom of the external structure are eliminated (see Appendix III) and boundary conditions applied. The stiffness equations are then expressed as

$$\left\{ \begin{array}{c} F_{uw\beta c\ell} \\ \hline F_{uw\beta cg} \end{array} \right\} = \left[K_c \right] \left\{ \begin{array}{c} u_{uw\beta c\ell} \\ \hline u_{uw\beta cg} \end{array} \right\} \tag{13}$$

Displacements u, w, β at all nodes in contact with both liquid and ullage gas are retained at this point the forces $\{F\}$ are total forces at a nodal circle which retains symmetry in the stiffness matrix.

LIQUID FREE SURFACE STIFFNESS ELEMENTS

In a uniform gravitational field the potential energy associated with liquid free surface displacements may be translated into an equivalent surface element stiffness. If a fluid element of cross-sectional area A is displaced a distance h above the mean free surface its potential energy is ρghA. The stiffness or spring constant of the element is then ρgA. Since these fluid elements are free to move independently of one another, the stiffness matrix of the liquid free surface is diagonal with stiffnesses proportional to element areas. Combining the container and free surface stiffness equations gives

$$\left\{ \begin{array}{c} F_{uw\beta c\ell} \\ \hline F_{uw\beta cg} \\ \hline F_s \end{array} \right\} = \left[K_c + K_s \right] \left\{ \begin{array}{c} u_{uw\beta c\ell} \\ \hline u_{uw\beta cg} \\ \hline u_s \end{array} \right\} \tag{14}$$

ULLAGE PRESSURE EFFECTS

Under time varying hydrodynamic pressures the elastic container will undergo small but finite volumetric changes. As a result, a nearly full tank containing ullage gas can experience significant percentage changes in ullage volume and hence ullage pressure. Such pressure variations can be treated by stiffness coefficients. Ullage pressure and ullage volume may be related by linearizing the pressure-volume relationship about the mean ullage volume V_o. Assuming an isentropic gas law the equation is

$$\Delta p = \gamma (P_o / V_o) \Delta V = B \Delta V \tag{15}$$

For each nodal circle displacement there is a corresponding volume change which can be derived as follows. Volume changes are first calculated for element displacements and are then combined appropriately at the nodes as are element stiffnesses to give a resultant nodal displacement volume change. A list of the formulas is given in Appendix II. To derive a so called pressure stiffness matrix for the ullage gas, it is convenient to think in terms of the physical significance of stiffness coefficients, that is, force required for a unit displacement and corresponding restraining forces. If ΔV_i is the volume change for nodal displacement $u_i = 1$, the pressure change throughout the ullage is $\Delta p_i = B \Delta V_i$. The equivalent concentrated nodal force for degree of freedom u_j is shown by Archer (Reference 6) to be given by

$$F_j = \int_s \Delta p_i \, \phi_j \, dS \tag{16}$$

where ϕ_j is the shape function for nodal displacement $u_j = 1$. But the $\int_s \phi_j \, dS$ is precisely ΔV_j. Therefore coefficients of the pressure stiffness matrix are given by $B \Delta V_i \, \Delta V_j$ where volume increases are positive.

The pressure matrix is full, that is, each degree of freedom on the ullage gas boundary couples with all others since the uniform pressure change is felt everywhere throughout the ullage volume. Liquid free surface displacements couple with container displacements at nodes in contact with the ullage. Combining the pressure stiffness matrix with $\left[K_c + K_s \right]$ we have

$$\left\{ \begin{array}{c} F_{uw\beta c\ell} \\ \hline F_{uw\beta cg} \\ \hline F_s \end{array} \right\} = \left[K_c + K_s + K_p \right] \left\{ \begin{array}{c} u_{uw\beta c\ell} \\ \hline u_{uw\beta cg} \\ \hline u_s \end{array} \right\} \tag{17}$$

Since the final stiffness matrix will contain only those displacement coordinates required to describe liquid motion, a series of force-free degree of freedom eliminations and a coordinate transformation are next performed. These steps are summarized below and the degrees of freedom remaining at the end of each step indicated. See also Appendix III.

1. Eliminate β degrees of freedom

$$\left\{ \begin{array}{c} u_{uwc\ell} \\ \hline u_{uwcg} \\ \hline u_s \end{array} \right\}$$

2. Eliminate u, w degrees of freedom at nodes in contact with the ullage gas.

$$\left\{ \begin{array}{c} u_{uwc\ell} \\ \hline u_s \end{array} \right\}$$

3. Transform u and w displacements to displacements tangent and normal to the container surface.

$$\left\{ \begin{array}{c} u_{tnc\ell} \\ \hline u_s \end{array} \right\}$$

4. Eliminate t degrees of freedom

$$\left\{ \begin{array}{c} u_{nc\ell} \\ \hline u_s \end{array} \right\}$$

The stiffness matrix at this point, denoted by $\left[K\right]$, contains only displacements normal to the container in liquid contact and the free surface displacements.

INCOMPRESSIBLE LIQUID CONSTRAINT

Due to fluid incompressibility not all of the degrees of freedom $\left\{ \begin{array}{c} u_{nc\ell} \\ \hline u_s \end{array} \right\}$ are independent. With each displacement u there is a volumetric change ΔV_u. The total liquid volume change ΔV_ℓ may then be expressed in matrix form by

$$\Delta V_\ell = \left\{\Delta V_u\right\}^T \left\{ \begin{array}{c} u_{nc\ell} \\ \hline u_s \end{array} \right\} \tag{18}$$

Note that ΔV_ℓ depends on all degrees of freedom u, w, β, u_s. Transformations required to obtain ΔV_u are given in Appendix III. Since $\Delta V_\ell = 0$ for liquid incompressibility, it is

convenient to introduce Δv_ℓ as a generalized coordinate and use the technique of generalized constraints proposed by Greene (Reference 7). Replacing the free surface displacement at the container centerline by Δv_ℓ, the coordinate transformation is written

$$\begin{Bmatrix} \underline{u}_{nc\ell} \\ \overline{u}_s \\ \Delta v_\ell \end{Bmatrix} = \left[\begin{array}{c|c} \mathbf{I} & 0 \\ \hline \{\Delta v_u\} & \end{array}\right] \begin{Bmatrix} \underline{u}_{nc\ell} \\ u_s \end{Bmatrix} \tag{19}$$

where $\overline{u}_s$ is u_s diminished by the centerline free surface displacement. Denoting the inverse of the square matrix above by $\mathbf{B}$ the required transformed stiffness matrix is

$$\left[\overline{K}\right] = \left[B\right]^T \left[K\right] \left[B\right] \tag{20}$$

Since the generalized coordinate Δv_ℓ is constrained to zero, the last row and column of $\overline{K}$ are deleted and the final stiffness equations of the system become

$$\begin{Bmatrix} \underline{F}_{nc\ell} \\ \overline{F}_s \end{Bmatrix} = \left[\overline{K}\right] \begin{Bmatrix} \underline{u}_{nc\ell} \\ \overline{u}_s \end{Bmatrix} \tag{21}$$

SECTION V

DERIVATION OF LIQUID MASS MATRIX

A finite element derivation of the fluid mass associated with its motion in an elastic container is presented in this section. This derivation is limited to liquids starting from a state of external and internal equilibrium. Under the assumptions that viscosity effects are negligible and the flow is irrotational, the fluid motion can be described by a velocity potential Φ. This potential is fully determined by the geometric configuration of the liquid mass. This potential is identified in that it must be harmonic with normal derivatives assuming assigned values on the boundaries.

A solution for the velocity potential is sought which can treat general axisymmetric systems which is geometrically compatible with the structural idealization of the container. The method selected reduces to the solution of the Neumann Problem, or the Second Boundary Value Problem. The solution of the Neumann Problem is constituted by a numerical solution of Fredholm's equation of the second kind. Welch (Reference 8) discusses in some detail the Neumann Problem including assumptions, limitations and methodology used to obtain numerical solutions. Kellogg and Lamb (References 11 and 10) provide the theoretical basis for this discussion while computational methods are discussed by Smith and Pierce (Reference 4) and Pogorzelski (Reference 9).

The method discussed and presented is completely general in principle and can be employed in three dimensional problems; however, only the axisymmetric system is discussed.

HYDRODYNAMIC INFLUENCE COEFFICIENTS

The hydrodynamic influence coefficients relating source strengths (densities), normal velocities, and the potential function over the boundary of a body of revolution are obtained by the methods outlined in Reference 4. The method reduces to numerical solution Fredholm's equation of the second kind,

$$\left(\frac{\partial \Phi}{\partial n}\right)_p = \pm 2\pi\sigma(p) + \iint \sigma(q)\,\frac{\partial}{\partial n}\,\frac{1}{r}\,dS. \qquad (22)$$

The normal velocity at boundary point, p, is equal to the sum of the individual contributions induced at p by the source distribution σ over the surface S. The surface of revolution is idealized into a system of conical frustums. The source density is assumed constant over

any given element. The boundary conditions are evaluated at the midpoints of the elements. The normal derivatives of $1/r$ are required and then the source distribution $\sigma(p)$ can be solved in terms of the known boundary conditions. The infinitesimal element is a homogeneous ring of which the potential and its derivatives are required. Let λ be the linear density (not a function of θ) and a the radius of the ring. The potential at point p in the x-y plane is given by

$$\Phi_p = 2a\lambda \int_0^{\pi} \frac{d\theta}{(x^2 + y^2 + a^2 - 2ay\cos\theta)^{1/2}} \tag{23}$$

The normal and tangential derivatives of the potential are obtained in terms of the cartesian velocity components (x and y directions) $\frac{\partial \Phi}{\partial x}$ and $\frac{\partial \Phi}{\partial y}$, respectively.

$$\frac{\partial \Phi}{\partial x} = -2a\lambda \int_0^{\pi} \frac{x\, d\theta}{(x^2 + y^2 + a^2 - 2ay\cos\theta)^{3/2}}$$

$$\frac{\partial \Phi}{\partial y} = -2a\lambda \int_0^{\pi} \frac{(y - a\cos\theta)\, d\theta}{(x^2 + y^2 + a^2 - 2ay\cos\theta)^{3/2}} \tag{24}$$

Define a coordinate s as the direction along the profile of the body of revolution from the point x_o, y_o to the point x_n, y_n, where (x_o, y_o) is the initial point defining the body (origin) and (x_n, y_n) is the last point of the body. The x axis is considered the axis of revolution. Divide the body into n conical frustums and define s_{2i-2}, s_{2i} to be the s coordinates of the end points of the i^{th} frustum (Figure 2). The cartesian coordinates of these points are

$$(\xi_{2i-2}, \eta_{2i-2}), (\xi_{2i}, \eta_{2i})$$

with midpoint

$$(\xi_{2i-1}, \eta_{2i-1}).$$

Define the angle α_i as the angle between the line tangent to the midpoint of the i^{th} frustum and the x axis, positive direction taken counterclockwise from the x axis. The expressions for the normal and tangential velocities are:

$$\left(\frac{\partial \Phi}{\partial n}\right)_{2i-1} = -2\pi\sigma_i - \sin\alpha_i \sum_{j=1}^{N} X_{ij}\,\sigma_j + \cos\alpha_i \sum_{j=1}^{N} Y_{ij}\,\sigma_j \tag{25}$$

$$\left(\frac{\partial \Phi}{\partial s}\right)_{2i-1} = \cos\alpha_i \sum_{j=1}^{N} X_{ij}\,\sigma_j + \sin\alpha_i \sum_{j=1}^{N} Y_{ij}\,\sigma_j \tag{26}$$

where

$$X_{\substack{ij \\ i \neq j}} = -4 \int_{s_{2j-2}}^{s_{2j}} \frac{\eta_j \, (x_{2i-1} - \xi_j) \, E(k) \, ds}{C_1 \, C_2} \tag{27}$$

$$Y_{\substack{ij \\ i \neq j}} = -2 \int_{s_{2j-2}}^{s_{2j}} \frac{\eta_j}{y_{2i-1} \, C_1} \left(K(k) + \cdot \frac{y_{2i-1}^2 - \eta_j^2 - (x_{2i-1} - \xi_j)^2}{C_2} E(k) \right) ds \tag{28}$$

$$C_1 = \left[(y_{2i-1} + \eta_j)^2 + (x_{2i-1} - \xi_j)^2 \right]^{1/2}$$

$$C_2 = (y_{2i-1} - \eta_j)^2 + (x_{2i-1} - \xi_j)^2$$

E(k) and K(k) are complete elliptic integrals of the first and second kind, respectively.

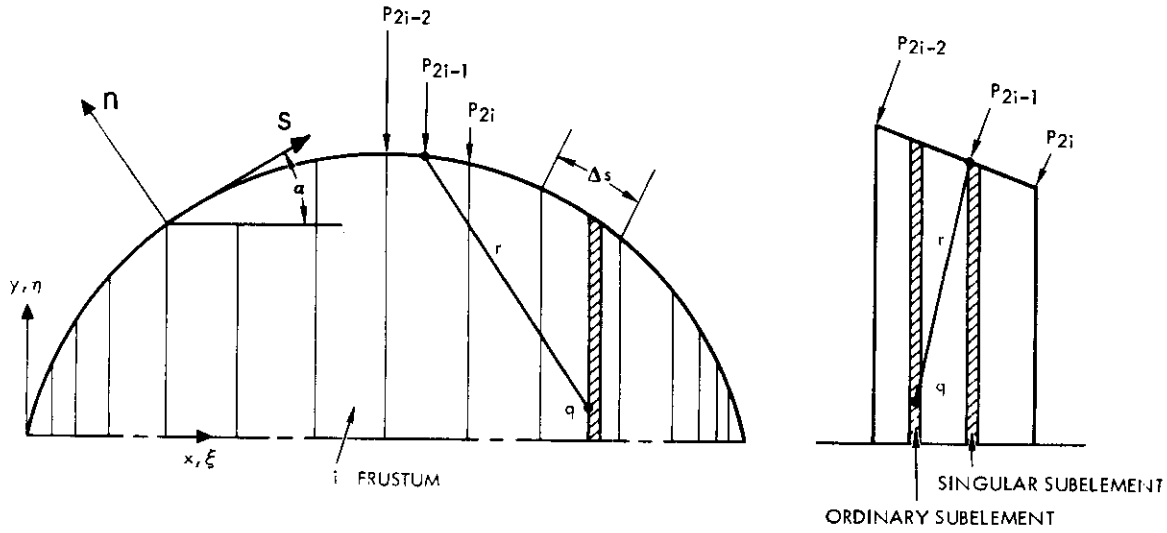

Figure 2. Configuration and Nomenclature for the Cone-Frustums Including Singular Subelement

The case of the ii element must be given special treatment, that is, the influence of a given element on itself. This particular element is divided into three parts by considering a small distance ϵ from the midpart of the element in each direction as defining the singular portion of the element. The integration of Equations 27 and 28 are performed over the intervals

$$(s_{2j-2},\ s_{2j-1}-\epsilon) \quad \text{and} \quad (s_{2j-1}+\epsilon,\ s_{2j}).$$

For the singular subelement let $2S'$ be the slant height of the element and then define a new coordinate as $S = s/y$. ($\epsilon_i = s\,y_{2i-1}$, S' = constant). Then the equations X_{ii} and Y_{ii} become

$$X_{ii} = 8 \sin\alpha_i \cos\alpha_i \left(\frac{S_i'}{4} + \frac{1}{96}\left(\mathrm{Ln}\left(\frac{S_i'}{8}\right) + \sin^2\alpha_i + \frac{13}{16}\right) S_i'^3 + \cdots \right)$$

$$- 4\int_{s_{2i-2}}^{s_{2i-1}\epsilon_i} X_{ij}\,ds - 4\int_{s_{2i-1}+\epsilon_i}^{s_{2i}} X_{ij}\,ds \qquad (i=j) \tag{29}$$

$$Y_{ii} = \left(2\sin^2\alpha_i + 2\,\mathrm{Ln}\left(\frac{S_i'}{8}\right) S_i' - \frac{1}{24}\left(4 + 3\,\mathrm{Ln}\left(\frac{S_i'}{8}\right) - 2\sin^2\alpha_i - 2\sin^4\alpha_i\right) S_i'^3 + \cdots \right)$$

$$- 2\int_{s_{2i-2}}^{s_{2i-1}-\epsilon_i} Y_{ij}\,ds - 2\int_{s_{2i-1}+\epsilon_i}^{s_{2i}} Y_{ij}\,ds \qquad (i=j) \tag{30}$$

Equations 27 to 30 are substituted into Equation 25, which can then be written

$$\{V_n\} = [A]\ \{\sigma\} \tag{31}$$

where v_n are the normal velocities at the midpoints of the elements, **A** is a matrix of geometrical coefficients relating the source densities σ of the elements to the normal velocities. σ are the source densities to be determined to satisfy the imposed boundary conditions. This Equation 31 is solved to obtain the σ by a Gauss Jordan complete pivoting method.

$$[A] = \left[+2\pi - \sin\alpha_i \sum_{j=1}^{N} X_{ij} + \cos\alpha_i \sum_{j=1}^{N} Y_{ij} \right] \tag{32}$$

Once the source strengths have been determined, the potential Φ can be evaluated from

$$\Phi_p = 2 \sum_{i=1}^{N} \sigma_i \int_{s_{2i-2}}^{s_{2i}} a\,ds \int_0^{\pi} \frac{d\theta}{(x^2 + y^2 + a^2 - 2ay\cos\theta)^{1/2}} \tag{33}$$

This equation can be rewritten into the form similar to that for $\frac{\partial \Phi}{\partial n}$ and $\frac{\partial \Phi}{\partial s}$

$$\Phi_p = 4 \sum_{i=1}^{N} \sigma_i \int_{s_{2i-2}}^{s_{2i}} \frac{\eta_j K(k)_{ds}}{C_i} + \Phi_p^i \tag{34}$$

Φ_p^i is the contribution to the velocity potential from the singular subelement;

$$\Phi_p^i = \sigma_i \left\{ 4 \, Ln(8) S' + \frac{1}{6}\left[1 - 2 \sin^2 \alpha_i - Ln(8) \left(\sin^2 \alpha_i + \frac{1}{2} \right) \right] S'^3 + \cdots \right\} \tag{35}$$

Equation 34 can then be rewritten into matrix form as

$$\{\Phi\} = [B] \{\sigma\} \tag{36}$$

where matrix B is defined to be

$$[B] = \left[4 \sum_{i,j=1}^{N} \int_{s_{2i-2}}^{s_{2i}} \frac{\eta_j K(k) ds}{C_i} + \Phi^i \right] \tag{37}$$

FINITE ELEMENT EQUATIONS OF LIQUID MOTION

The pressure equation for incompressible, inviscid, irrotational flow under conservative forces is

$$\frac{p}{\rho} + \frac{1}{2} \nabla\Phi \cdot \nabla\Phi - \Omega - \frac{\partial \Phi}{\partial t} = f(t) \tag{38}$$

If there are no body forces and only small displacements are considered, the governing pressure equation becomes

$$\frac{p}{\rho} = \frac{\partial \Phi}{\partial t} \tag{39}$$

This is the equation for pressure at any point on the fluid. To obtain the total force exerted on any segment of the boundary the pressure is integrated over the surface.

Compatibility between the structural motion and fluid motion is achieved by equating total forces at the boundary. This entails integrating the pressure equation for the fluid over the individual elemental frusta that are employed in the idealization of the problem. The pressure forces acting on the fluid boundaries can be written as

$$F = \rho \iint \frac{\partial \Phi}{\partial t} \, dS \tag{40}$$

$$\{\Phi\} = [B] \{\sigma\} = [B] [A]^{-1} \{v_n\} \tag{41}$$

$$\left\{ \frac{\partial \Phi}{\partial t} \right\} = [B] [A]^{-1} \{\dot{v}_n\} \tag{42}$$

This expression is valid since the matrices **B** and **A** are geometrical constants. The force equation can then be written in matrix form as

$$\{F\} = \rho [S][B][A]^{-1}\{\dot{v}_n\} \tag{43}$$

where the matrix **S** is an integrating matrix for the respective fluid elements which match the structural elements. **S** is a banded matrix whose band width is dependent upon the degree of sophistication one wishes to use for the integrating scheme. The mass matrix is identified as

$$[M] = \rho [S][B][A]^{-1} \tag{44}$$

The mass matrix can also be identified from a kinetic energy expression. The kinetic energy of the fluid in terms of the velocity potential is

$$T = \frac{\rho}{2} \int\int \Phi \frac{\partial \Phi}{\partial n} dS \tag{45}$$

Substituting into Equation 45 the matrix expressions for Φ and $\frac{\partial \Phi}{\partial n}$ from Equations 31 and 41 and the equivalent numerical expression for integration, one obtains

$$T = \frac{\rho}{2} \left\{\frac{\partial \Phi}{\partial n}\right\}^T [S][\Phi] = \frac{\rho}{2} \{v_n\}^T [S][B][A]^{-1}\{v_n\} \tag{46}$$

The proof of symmetry of the analytical expression used in the matrix approximation of the mass is given in Appendix IV. This proof is due to Professor Tong (Reference 12).

SECTION VI

A NUMERICAL EXAMPLE

A computer program based on the problem formulation presented here was written for the IBM 360/65 computer. This program is sized for a total of 80 elements over the shell and free surface. It has demonstrated machine running times of about seven minutes for a 43-element system, including digital and graphical output of all system frequencies and mode shapes.

To substantiate validity of this problem formulation, an example has been selected from the literature, and compared with the finite element solution. The problem is that of a filled hemispherical shell, simply supported at the equator. Tai and Uchiyama (Reference 13) investigated this configuration and obtained numerical results for the following geometric and structural properties:

Radius	= 200 inches
Shell thickness	= 0.1 inch
Elastic Modulus	= 10^7 psi
Structural mass density	= $2.59 \times 10^{-4} \frac{\text{lbs sec}^2}{\text{in}^4}$
Poisson's ratio	= 0.3
Fluid density (LOX)	= $1.06 \times 10^{-4} \frac{\text{lbs sec}^2}{\text{in}^4}$

Natural frequencies obtained by the finite element program (neglecting wall mass) for the 43-element, 42-degrees-of-freedom system are shown as circular symbols along a logarithmic scale in Figure 3. The four natural frequencies computed by Tai and Uchiyama are also indicated in Figure 3. Their first mode is shown to be considerably below the lowest frequency obtained by the finite element program. On the other hand, the remaining three frequencies show reasonable agreement with those for the lowest structural modes obtained by the finite element program. The connecting dashed lines indicate corresponding frequencies based upon inspection of the number of nodal points in the mode shapes.

The large number of frequencies indicated below the first structural mode at 6.7 Hz are all associated with modes having predominantly free surface motion.

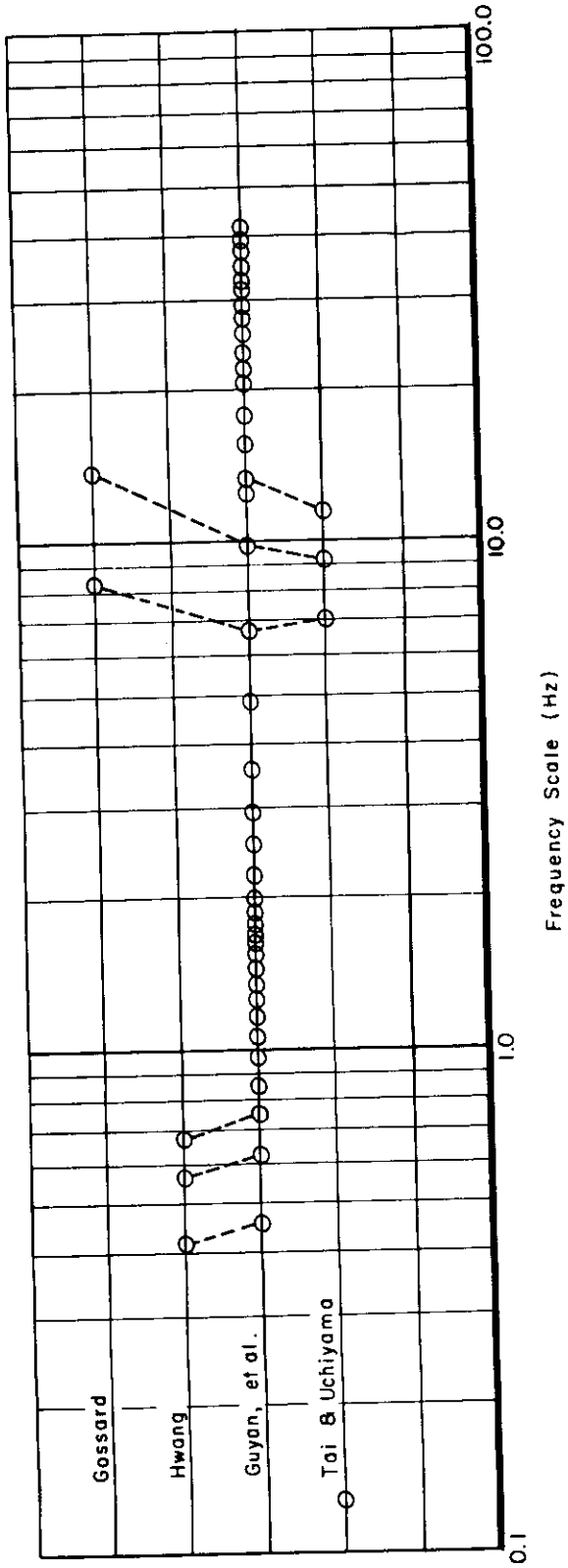

Figure 3. Frequency Correlation

The technique employed by Tai and Uchiyama for solution of the frequency determinant consisted of a trial and correction searching process for the zeroes. This explains, at least in part, why some of the frequencies below those for the structural modes appear to have been missed.

In an effort to resolve the discrepancy at the fundamental free surface frequency, it was noted that the frequency ratio between the fundamental free surface frequency and the first structural frequency computed by the finite element program is 0.46 to 6.7 or about 1 to 15. For such a spread, it may be concluded that structural participation is negligible for the first free surface mode. This is further substantiated by the mode shape. Its response must essentially be that for a rigid container. Hwang (Reference 14) analyzed this same configuration except that he used a wall thickness of 0.3 inches. By the preceding argument this larger thickness would not change the magnitude of fundamental free surface frequency from that for 0.1 inch wall thickness. The value of 0.42 Hz which he obtained for this frequency is indicated in Figure 3. Hwang also calculated two higher slosh mode frequencies for the hemispherical tank. Comparison with these frequencies is indicated in Figure 3.

Gossard (Reference 15) solved the free vibration problem for the same configuration with one notable exception. His model assumed a rigid ring at the equatorial support whose mass was taken to be equal to that of the fluid. The system was otherwise unsupported. The two structural frequencies determined by Gossard for his model are shown in Figure 3. As might be expected, these frequencies are higher than those for the corresponding modes computed by the finite element program.*

The finite element program computed all the mode shapes for the sample problem. For the assumed structural and fluid properties a rather distinct separation occurred between the free surface and structural modes.

---

*Mr. Gossard, in his investigation, did study the frequencies for a hemisphere with the equatorial ring completely restrained from motion along the axis. The lowest frequency he obtained, however, was higher than the corresponding fundamental with the ring unrestrained. This is contrary to the trend exhibited by a simple double mass-spring system. For this simple system the frequency is known to decrease when one mass is fixed (or made infinitely heavy). One of the authors questioned Mr. Gossard on this point, and he stated that the point was well taken. He felt that his fixed equator result required further substantiation. His solution for the unsupported case was considered correct on the basis of its correlation with independent data as shown in his report.

Figures 4, 5 and 6 show the first three modes of the hemispherical shell, which are seen to be sloshing modes. Figure 7 shows the first 21 characteristic free surface wave shapes in order of increasing natural frequency. Only the wave shape along the radius is shown since the motion is axisymmetric. With the maximum wave amplitude normalized to unity, the maximum wall displacements for these modes are on the order of 10^{-4} or less. Therefore the wall participation is essentially negligible, and these modes are characterized as free surface modes. From the standpoint of linearized dynamics their existence is primarily of academic interest, since they would presumably be difficult to excite. Nevertheless, the progressive manner with which the higher frequency characteristics gradually make themselves evident with increasing frequency is interesting. The most noticeable of these frequency dependent features are (a) the steady increase in number of nodal points from mode 1 to mode 14, (b) the appearance of a localized, highly oscillatory wave shape at the center in mode 13, which appears to move steadily outward with increasing frequency, leaving a relatively calm surface towards the center. Figures 8, 9, and 10 show the succeeding mode shapes corresponding to the 22nd, 23rd, and 24th ascending frequencies. These are the first predominantly structural modes. Here also, as well as in all the remaining modes, the localized, highly oscillatory wave shape now located near the periphery continues to persist. No new features appear in the 25th and subsequent mode shapes except that nodal points along the wall steadily increase in number with increasing frequency. Obvious limitation to the numerical accuracy is indicated when the nodal points become so numerous that only one or two elements appear between nodal points of the deformation pattern. This deficiency became apparent at approximately the 34th mode. In the computer solution, the last three frequencies of the 42-degrees-of-freedom system were complex, indicating complete degeneration of numerical accuracy.

Upon viewing the entire set of mode shapes in order of increasing frequency, it is apparent that higher frequency fluctuations in the free surface, compatible with the structural modes, can have only limited representation due to the finite number of elements. This computer program has not yet undergone extensive usage, and limitations such as this have yet to be optimally resolved.

Versatility of this eigenproblem formulation is not fully demonstrated by a single numerical example. Suffice it to note that the characteristic generality of finite element techniques has essentially been preserved. The reasonable comparisons obtained with independently obtained data substantiate validity of the basic formulation.

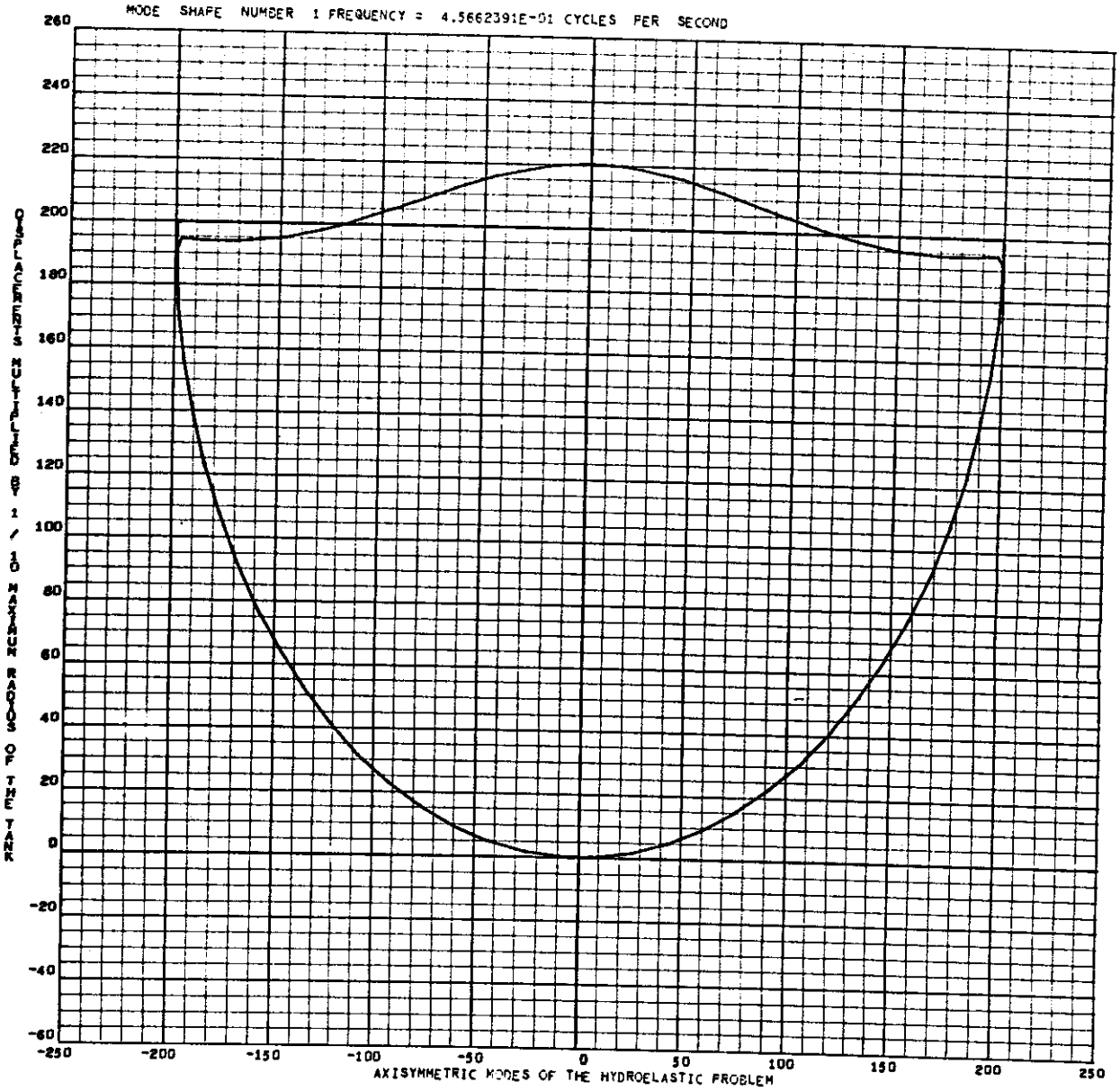

Figure 4. First Free Surface Mode, First System Mode

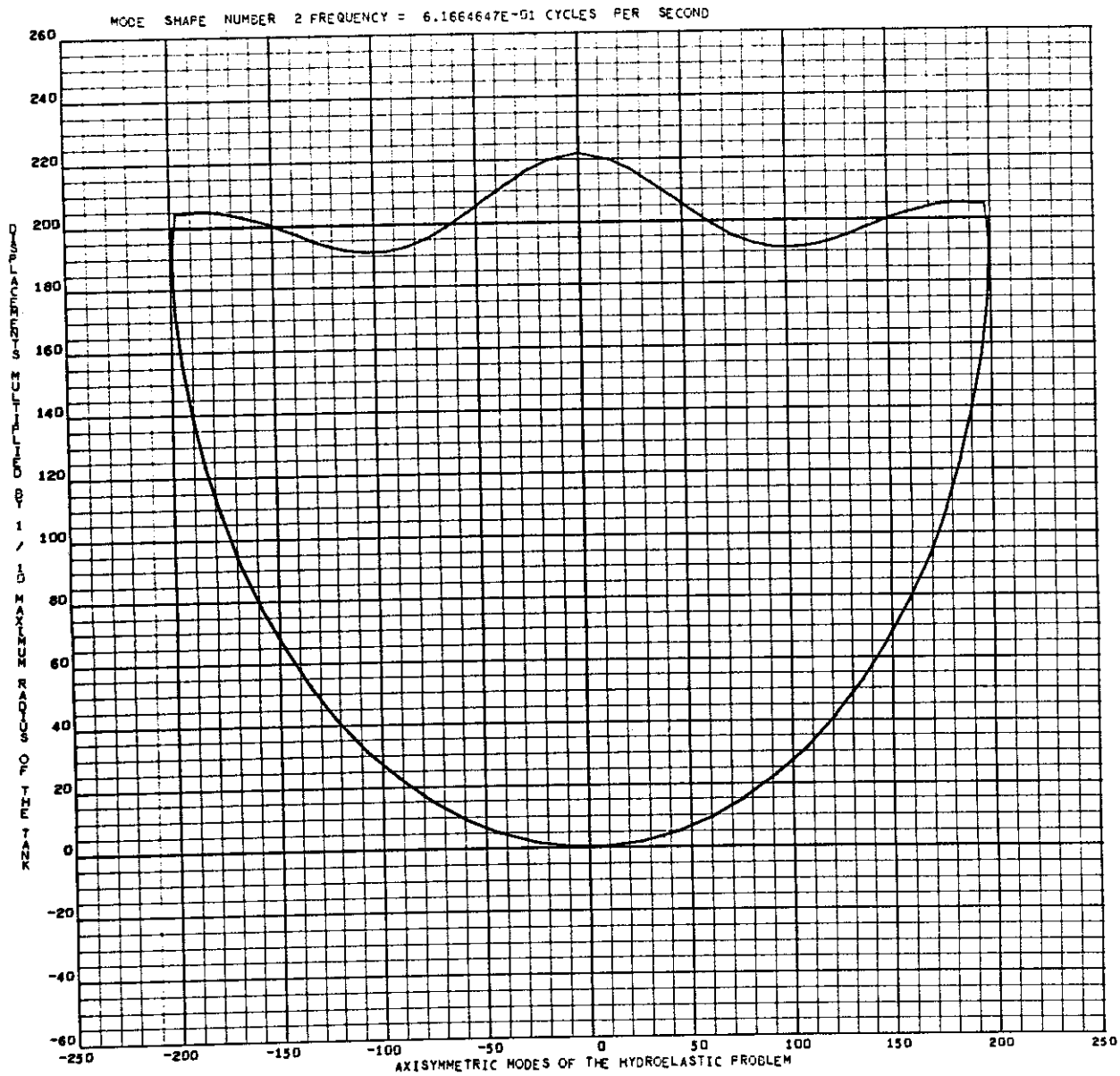

Figure 5. Second Free Surface Mode, Second System Mode

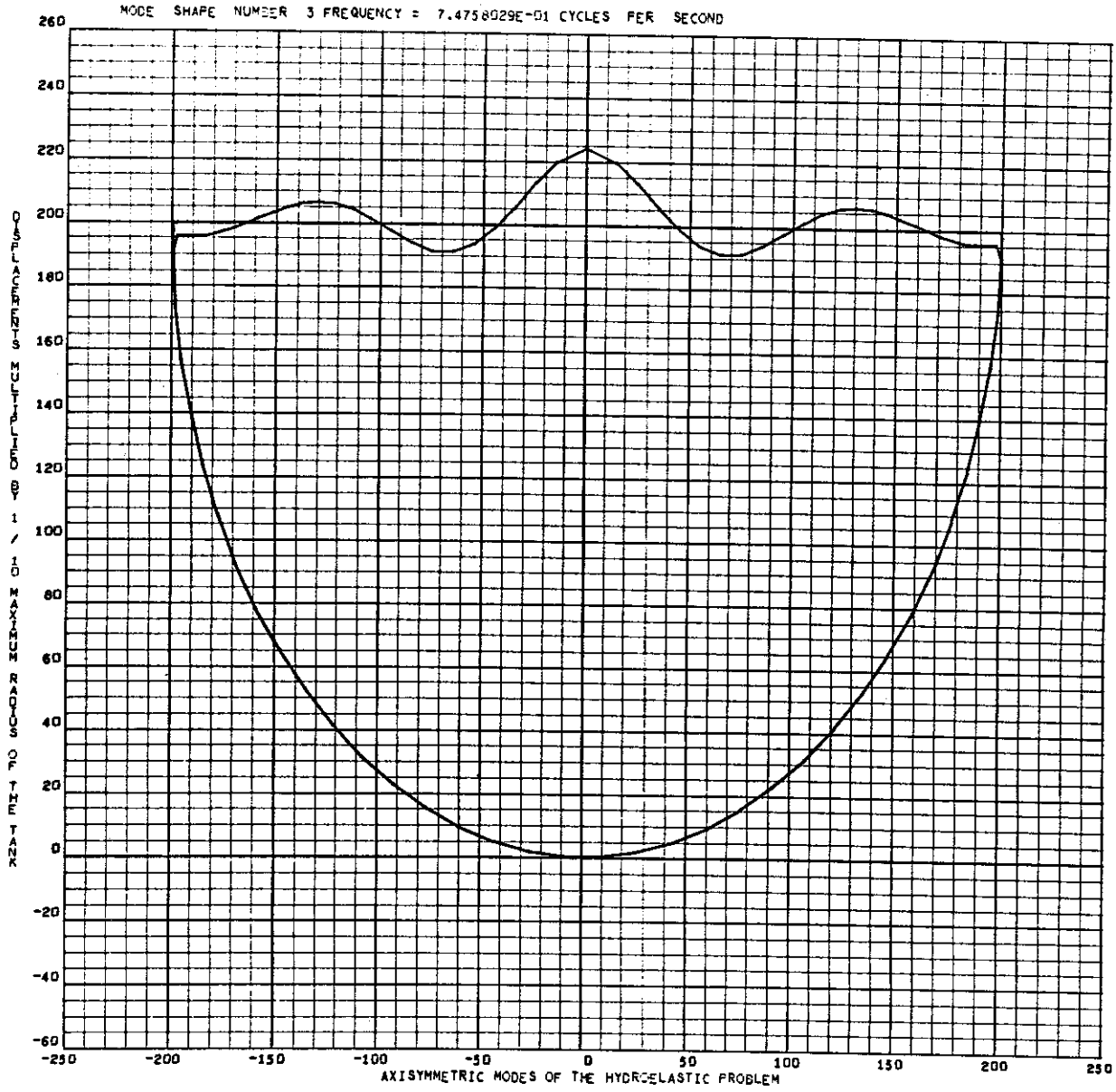

Figure 6. Third Free Surface Mode, Third System Mode

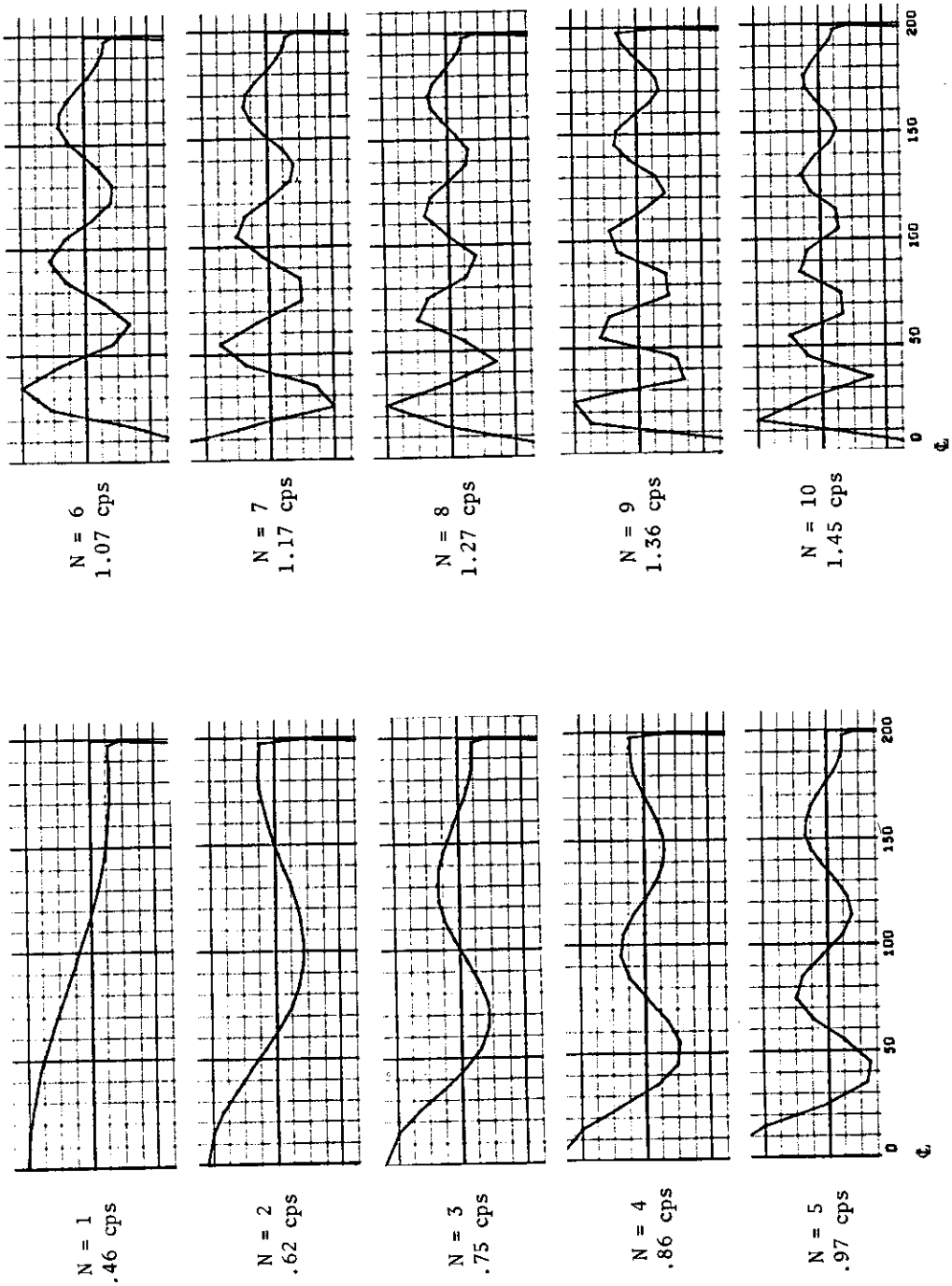

Figure 7. Axisymmetric Liquid Free Surface Wave Shapes for the First 21 Slosh Modes

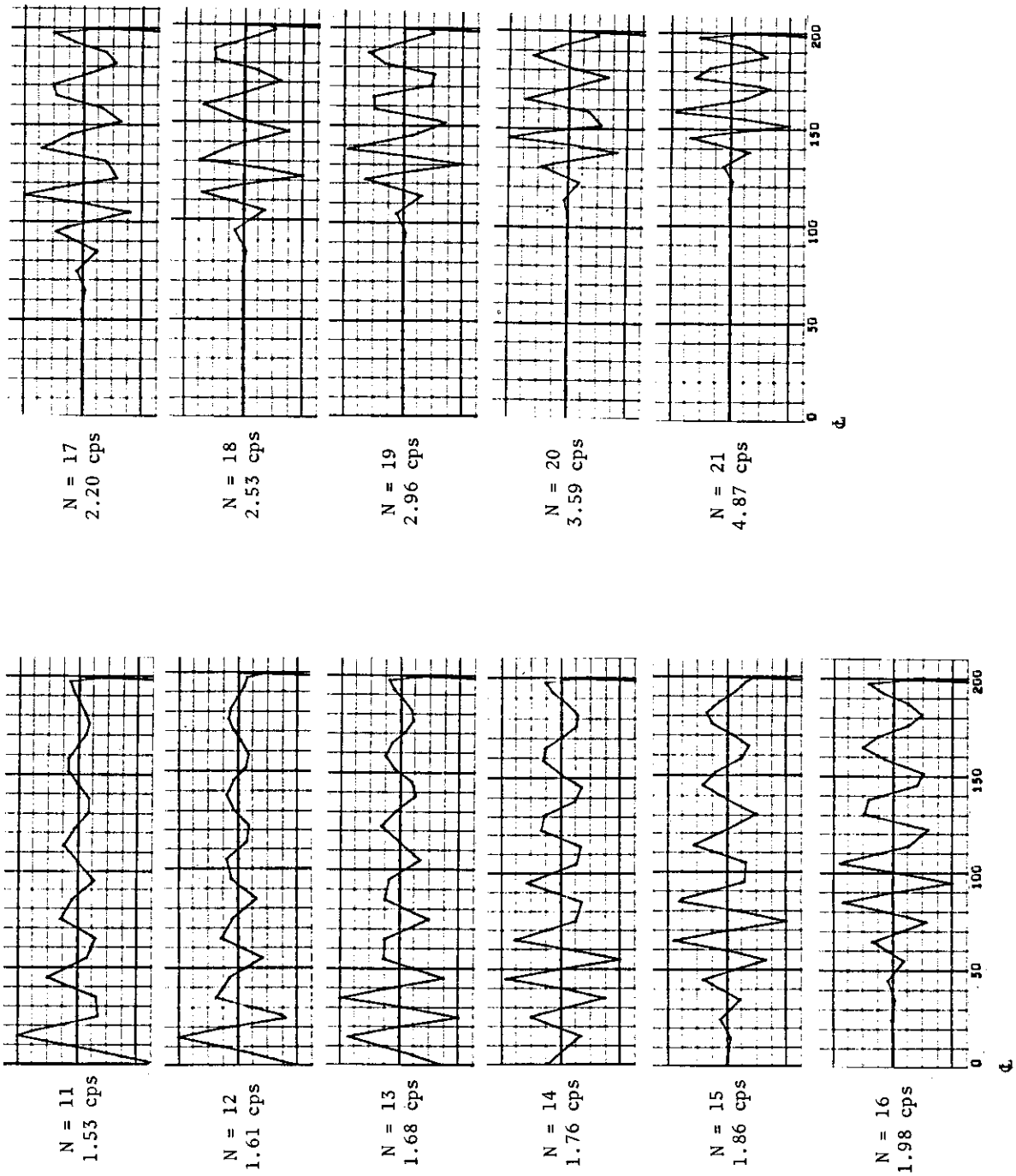

Figure 7 (completed)

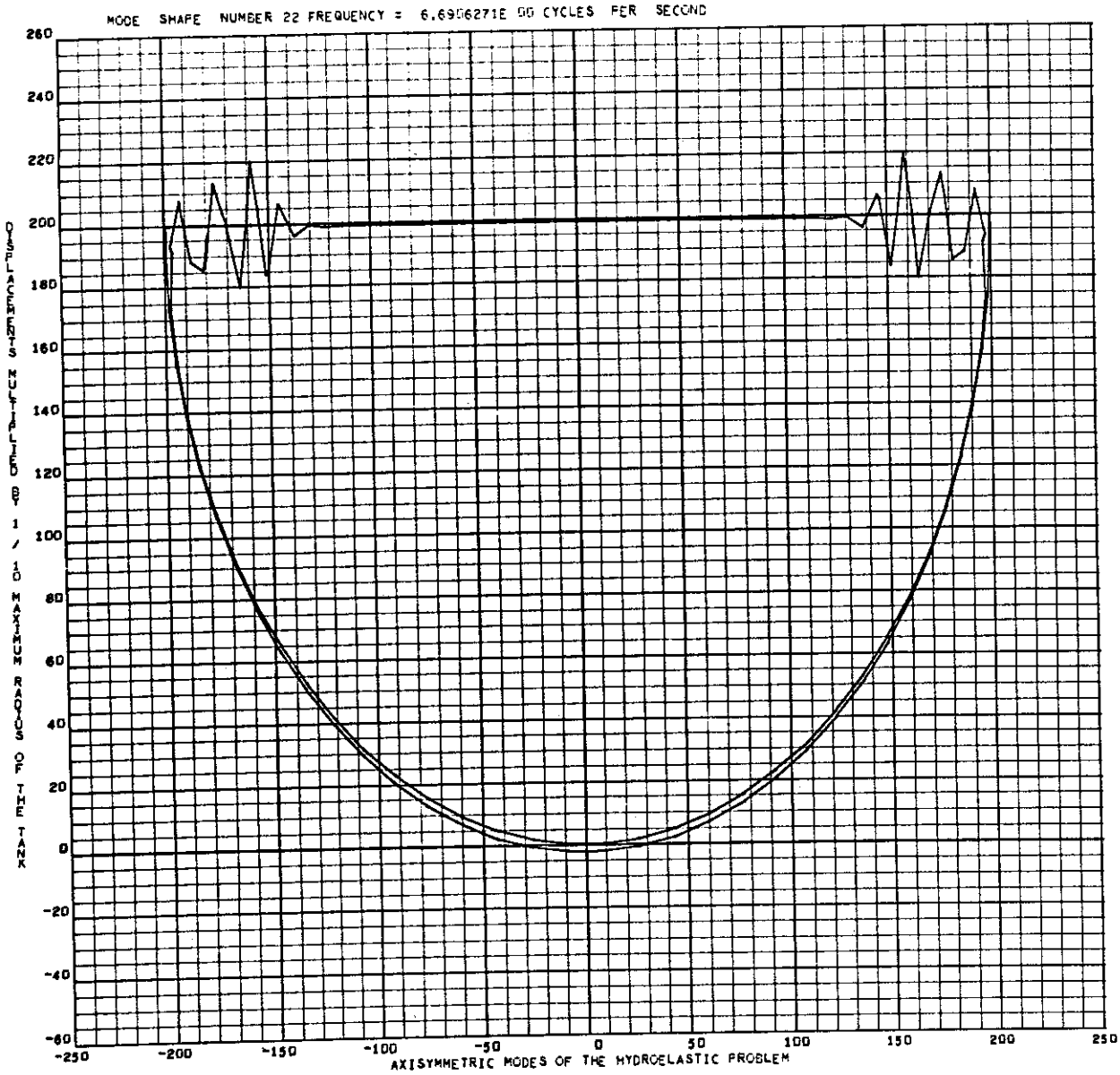

Figure 8. First Structural Mode, 22nd System Mode

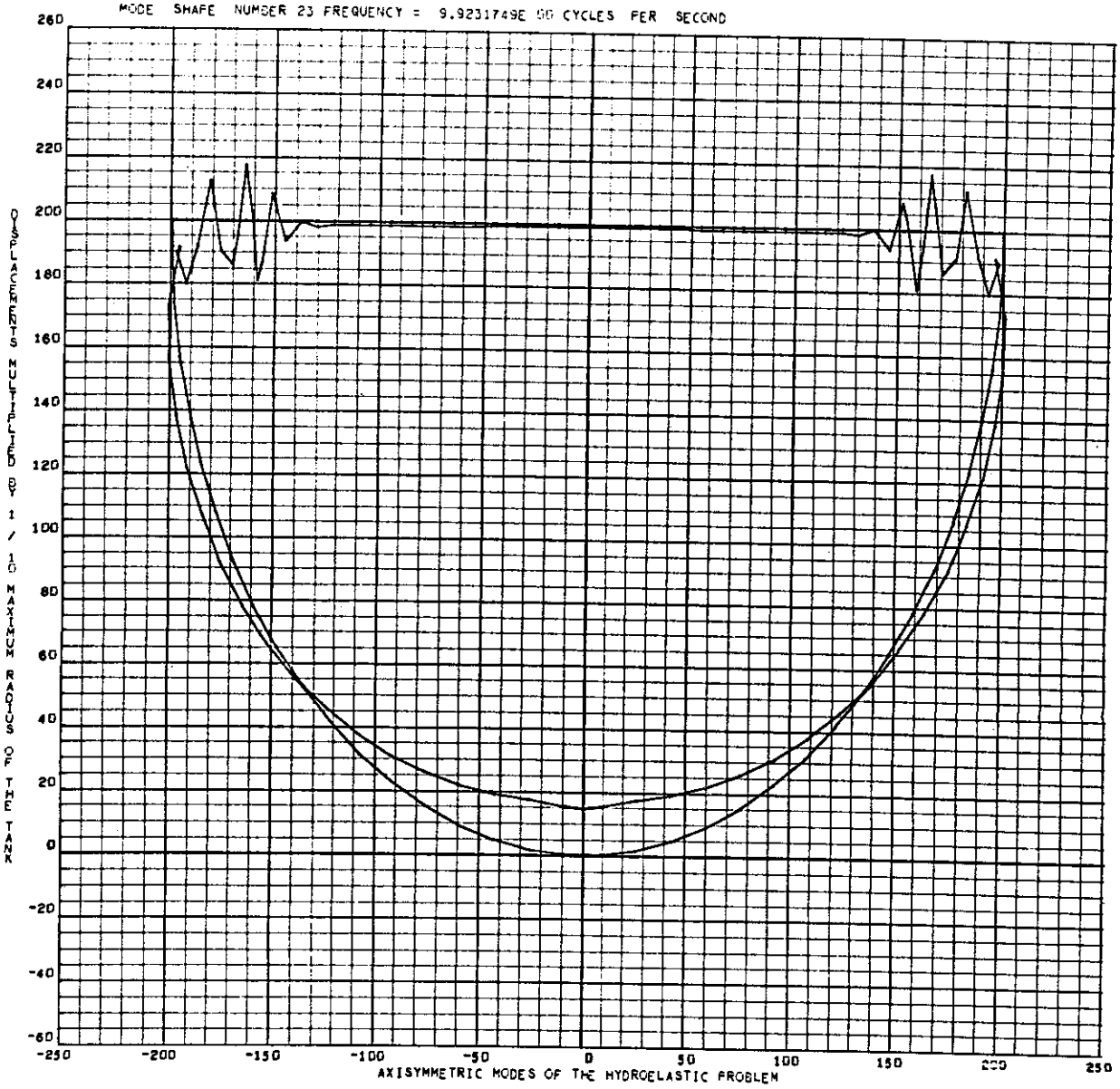

Figure 9. Second Structural Mode, 23rd System Mode

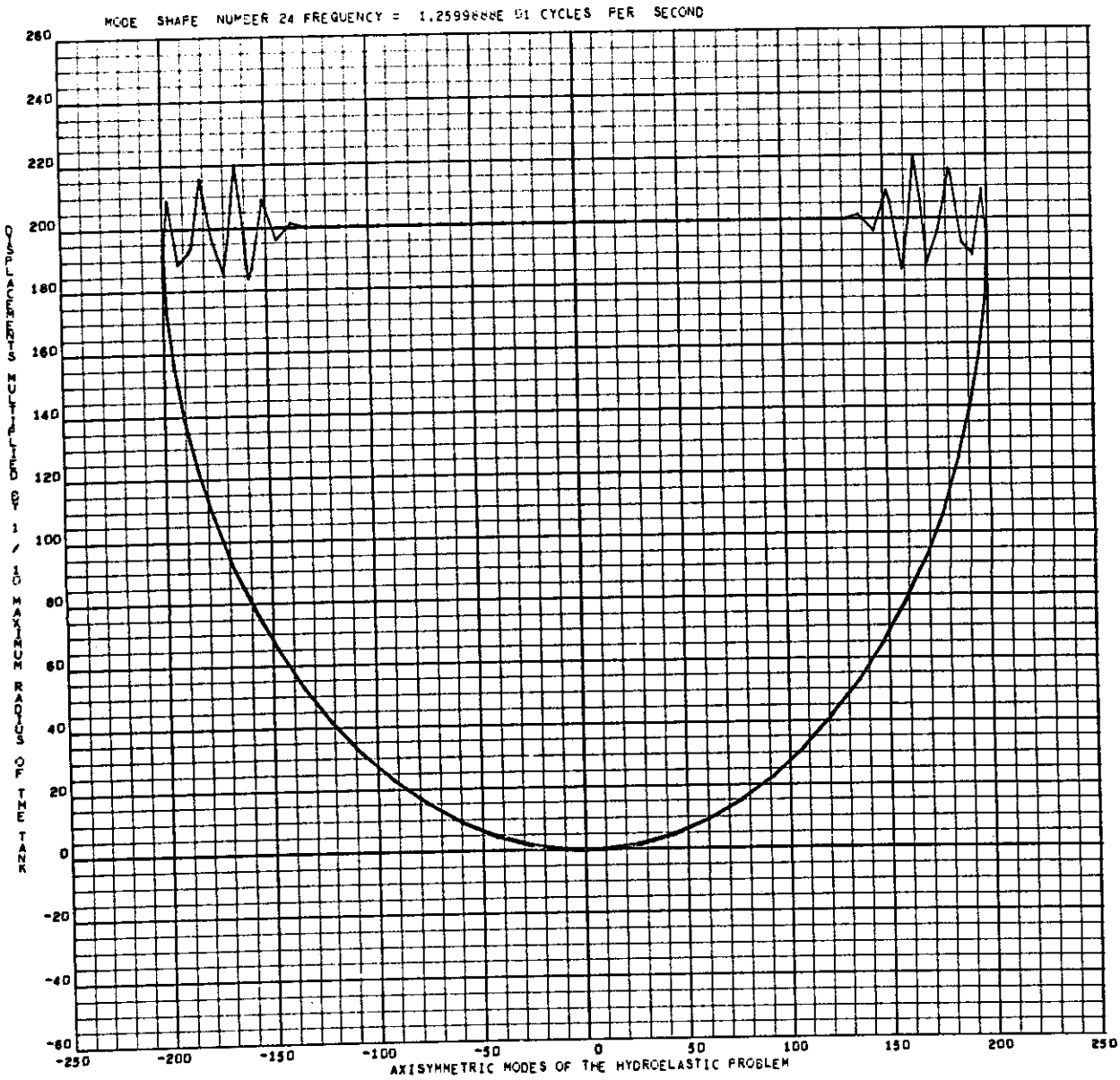

Figure 10. Third Structural Mode, 24th System Mode

SECTION VII

CONCLUSIONS

A method for hydroelastic analysis of axisymmetric systems by a finite element method has been demonstrated. Essentially, existing numerical analysis techniques have been adapted and combined to meet the requirements for solution of this hydroelastic system eigenproblem. In addition, the representation of the fluid free surface as a consistently defined structural boundary has been proposed. Ullage pressure effects and liquid incompressibility have been included in the stiffness formulation. Reasonable agreement with existing data has substantiated validity of the approach.

SECTION VIII

REFERENCES

1. Zienkiewicz, O. C., and Y. K. Cheung. The Finite Element Method in Structural and Continuum Mechanics, McGraw Hill Publishing Company Limited (1967).

2. Palmer, J. H., and G. W. Asher. "Calculation of Axisymmetric Longitudinal Modes for Fluid-Elastic Tank-Ullage Gas Systems and Comparison with Modal Results," Volume of Technical Papers presented at AIAA Symposium on Structural Dyamics and Aeroelasticity, Boston, Massachusetts (1965).

3. Tong, P. Liquid Sloshing in an Elastic Container, AFOSR 66-0943 (June 1966).

4. Smith, A. M. O., and J. Pierce. Exact Solution of The Calculation of Non-Circulatory Plane and Axially Symmetric Flows About or Within Arbitrary Boundaries, Douglas Aircraft Company, Inc., Report ES 26988 (April 1958).

5. Grafton, P. E., and D. E. Strome. "Analysis of Axisymmetrical Shells by the Direct Stiffness Method," AIAA Journal, Volume 1, Number 10 (October 1963).

6. Archer, J. S. "Consistent Matrix Formulations for Structural Analysis Using Finite-Element Techniques," AIAA Journal, Volume 3, Number 10 (October 1965).

7. Greene, B. E. "Application of Generalized Constraints in the Stiffness Method of Structural Analysis," AIAA Journal, Volume 4, Number 9 (September 1966).

8. Welch, P. W. Finite Element Analysis of Axisymmetric Steady Flows, North American Rockwell Corporation, STR 203 (April 1968).

9. Pogorzelski, W. Integral Equations and Their Applications, Vol. 1, Pergamon Press (1966).

10. Lamb, Sir Horace. Hydrodynamics, Dover Publications, New York (1945).

11. Kellogg, O. D. Foundations of Potential Theory, Dover Publications, New York (1953).

12. Tong, P. Symmetric Equivalent Mass Matrix for the Fluid in the Liquid Sloshing Problem, (1968). (Correspondence between Professor Tong and the authors.)

13. Tai, Clement L., and Shoichi Uchiyama, "A New Approach to the Interaction Problems of Fluid-Filled Elastic Membrane Shells," presented at 38th Shock and Vibration Symposium, St. Louis, Missouri, April 29 - May 1, 1968.

14. Hwang, C., "Longitudinal Sloshing of Liquid in a Flexible Hemispherical Tank," J. Applied Mechanics, Paper No. 65-APM-14, 1965.

15. Gossard, M. L. "Axisymmetric Dynamic Response of Liquid-Filled, Hemispherical, Thin-Walled, Elastic Tanks," Volume of Technical Papers presented at AIAA Symposium on Structural Dynamics and Aeroelasticity, Boston, Massachusetts (1965).

APPENDIX I

CIRCULAR PLATE STIFFNESS EQUATIONS

A three-degrees-of-freedom circular plate element is used at the container centerline to match the adjoining conical element displacements. The generalized forces are force per unit length multiplied by $2\pi a$.

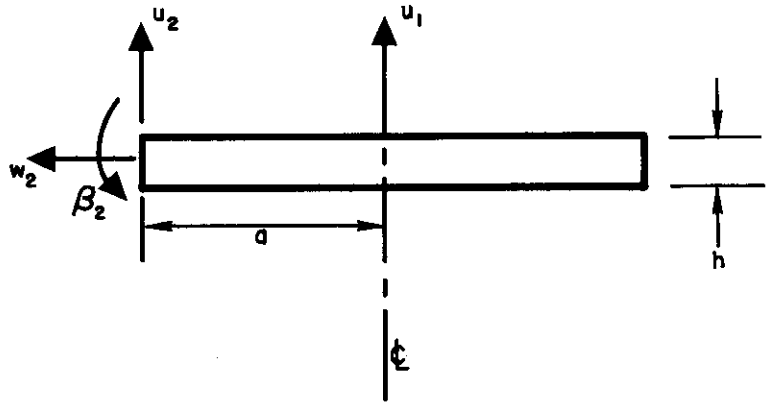

Circular Plate Element

$$\begin{bmatrix} F_{u_2} \\ F_{w_2} \\ F_{\beta_2} \end{bmatrix} = \begin{bmatrix} 0 & 0 & 0 \\ 0 & \frac{2\pi Eh}{1-\nu} & 0 \\ 0 & 0 & \frac{\pi Eh^3}{6(1-\nu)} \end{bmatrix} \begin{bmatrix} u_2 \\ w_2 \\ \beta_2 \end{bmatrix} \tag{47}$$

The center displacement is given by

$$u_1 = u_2 + \frac{a}{2}\beta_2 \tag{48}$$

APPENDIX II

STRUCTURAL ELEMENT VOLUME CHANGES

Container volume changes associated with the conical frustum element displacements are easily calculated by use of a theorem of Pappus. Element displacements are made one at a time with all others restrained to zero. The deformed element and generating area for w_1 is shown in the figure. An increase in volume is positive.

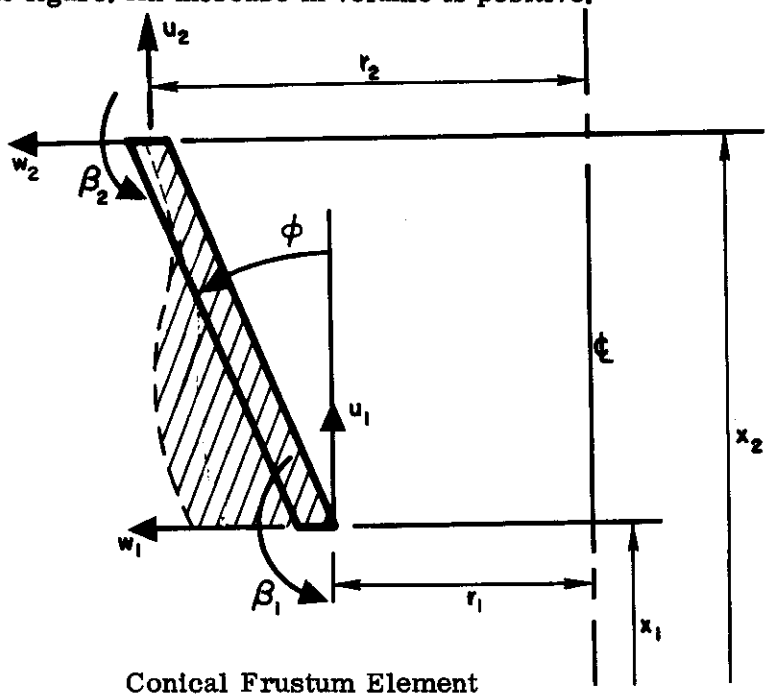

Conical Frustum Element

$$\Delta V_{u_1} = -\pi\left[r_1 + (r_2 - r_1)\left(\frac{1}{3} - \frac{1}{30}\cos^2\phi\right)\right](r_2 - r_1)\,u_1 \tag{49}$$

$$\Delta V_{w_1} = \pi\left[r_1 + (r_2 - r_1)\left(\frac{1}{3} - \frac{1}{30}\cos^2\phi\right)\right](x_2 - x_1)\,w_1 \tag{50}$$

$$\Delta V_{\beta_1} = \frac{\pi}{6}\left(\frac{3}{5}r_1 + \frac{2}{5}r_2\right)(x_2 - x_1)^2\,\beta_1 \tag{51}$$

$$\Delta V_{u_2} = -\pi\left[r_1 + (r_2 - r_1)\left(\frac{2}{3} + \frac{1}{30}\cos^2\phi\right)\right](r_2 - r_1)\,u_2 \tag{52}$$

$$\Delta V_{w_2} = \pi\left[r_1 + (r_2 - r_1)\left(\frac{2}{3} + \frac{1}{30}\cos^2\phi\right)\right](x_2 - x_1)\,w_2 \tag{53}$$

$$\Delta V_{\beta_2} = -\frac{\pi}{6}\left(\frac{2}{5}r_1 + \frac{3}{5}r_2\right)(x_2 - x_1)^2\,\beta_2 \tag{54}$$

Volume changes for the circular plate shown in Appendix I are

$$\Delta V_{u_2} = \pm \pi a^2 u_2 \tag{55}$$

$$\Delta V_{\beta_2} = \pm \frac{\pi a^3}{4} \beta_2 \tag{56}$$

The negative sign applies at the container bottom and the positive sign at the top.

For the free surface elements, the changes are simply

$$\Delta V_{u_s} = \pi (r^2_{outer} - r^2_{inner}) u_s \tag{57}$$

APPENDIX III

COORDINATE TRANSFORMATIONS FOR VOLUME CHANGES

Since all modal displacements give rise to container volume change, the contribution of each must be included at the stage in the calculations when the constant volume constraint is imposed. As degrees of freedom are eliminated coordinate transformations are obtained as follows.

$$\left\{\begin{array}{c} F_1 \\ \hline F_2 \end{array}\right\} = \left[\begin{array}{c|c} K_{11} & K_{12} \\ \hline K_{21} & K_{22} \end{array}\right] \left\{\begin{array}{c} u_1 \\ \hline u_2 \end{array}\right\} \tag{58}$$

The $\{u_1\}$ are to be eliminated by setting $\{F_1\} = 0$.

Then

$$\{u_1\} = -\left[K_{11}^{-1} K_{12}\right]\{u_2\} \tag{59}$$

and

$$\left\{\begin{array}{c} u_1 \\ \hline u_2 \end{array}\right\} = \left[\begin{array}{c} K_{11}^{-1} K_{12} \\ \hline I \end{array}\right]\{u_2\} \tag{60}$$

gives the form of the transformation required.

For the eliminations and transformation indicated in the main text, the equations follow.

For the β elimination,

$$\left\{\begin{array}{c} u_{uw\beta c\ell} \\ \hline u_{uw\beta cg} \\ \hline u_s \end{array}\right\} = \left[T_1\right] \left\{\begin{array}{c} u_{uwc\ell} \\ \hline u_{uwcg} \\ \hline u_s \end{array}\right\} \tag{61}$$

$[T_1]$ is constructed by an arrangement of the matrix relating β and u, w displacements and an identity matrix which accounts for reordering of the displacements.

Eliminating u_{uwcg}

$$\left\{\begin{array}{c} u_{uwc\ell} \\ \hline u_{uwcg} \end{array}\right\} = \left[T_2\right] \left\{\begin{array}{c} u_{uwc\ell} \\ \hline u_s \end{array}\right\} \tag{62}$$

Transforming from u, w to t, n,

$$\left\{\frac{u_{uwc\ell}}{u_s}\right\} = \left[\begin{array}{c|c} \mathbf{B} & \\ \hline & \mathbf{I} \end{array}\right] \left\{\frac{u_{tnc\ell}}{u_s}\right\} \tag{63}$$

Elements of $\mathbf{B}$ are the direction cosines of the container surface tangent and normal.

Eliminating $u_{tc\ell}$

$$\left\{\frac{u_{tnc\ell}}{u_s}\right\} = \left[T_3\right] \left\{\frac{u_{nc\ell}}{u_s}\right\} \tag{64}$$

Combining these equations, we arrive at the overall transformation

$$\left\{\begin{array}{c} \frac{u_{uw\beta c\ell}}{u_s} \\ \hline \frac{u_{uw\beta cg}}{u_s} \end{array}\right\} = \left[T_1\right] \left[T_2\right] \left[\begin{array}{c|c} \mathbf{B} & \\ \hline & \mathbf{I} \end{array}\right]$$

$$\left[T_3\right] \left\{\frac{u_{nc\ell}}{u_s}\right\} = \left[T\right] \left\{\frac{u_{nc\ell}}{u_s}\right\} \tag{65}$$

Now construct a liquid volume change matrix $\{\Delta\mathbf{V}\}$ by superposition of the element volume changes given in Appendix II. Then

$$\Delta V_\ell = \{\Delta\mathbf{V}\}^T \left\{\begin{array}{c} \frac{u_{uw\beta c\ell}}{u_s} \\ \hline \frac{u_{uw\beta cg}}{u_s} \end{array}\right\} \tag{66}$$

In terms of the displacements remaining when fluid incompressibility is enforced

$$\Delta V_\ell = \{\Delta\mathbf{V}\}^T \left[T\right] \left\{\frac{u_{nc\ell}}{u_s}\right\} = \{\Delta\mathbf{V}_u\}^T \left\{\frac{u_{nc\ell}}{u_s}\right\} \tag{67}$$

APPENDIX IV

SYMMETRY OF THE MASS MATRIX

The following proof of the symmetry of the analytical expression for the mass matrix is due to Professor Tong, and is referenced in the main text.

$$T = -\frac{\rho}{2}\iint \Phi\frac{\partial\Phi}{\partial n}\,ds \tag{68}$$

$$\Phi(p) = \iint \frac{H(q)}{r(p,q)}\,ds(q) \tag{69}$$

$$\frac{\partial\Phi}{\partial n}(p) = 2\pi H(p) + \iint H(q)\frac{\partial}{\partial n(p)}\frac{1}{r(p,q)}\,ds(q) \tag{70}$$

H(q) is an unknown function (source density)

n is the normal direction

p,q are points on the surface

r(p,q) is distance between p and q.

Substituting into the expression for the kinetic energy, one obtains

$$T = -\frac{\rho}{2}\iint\left[\iint\frac{H(q)}{r(p,q)}\,ds(q)\right]\left[2\pi H(p) + \iint H(q)\frac{\partial}{\partial n(p)}\frac{1}{r(p,q)}\,ds(q)\right]ds(R) \tag{71}$$

or

$$T = -\frac{\rho}{2}\iint\left[\iint H(p)\,F(p,q)\,H(q)\,ds(p)\right]ds(R) \tag{72}$$

where

$$F(p,q) = \frac{2\pi}{r(p,q)} + \iint\frac{1}{r(p,q)}\frac{\partial}{\partial n(p)}\frac{1}{r(p,q)}\,ds(p) \tag{73}$$

One can show F(p,q) = F(q,p).

$$\Phi_{1,2}(p) = \iint\frac{H_{1,2}(q)}{r(p,q)}\,ds(q) \tag{74}$$

so

$$\iint\Phi_1(p)\frac{\partial\Phi_2(p)}{\partial n}\,ds = \iiint\nabla\Phi_1\cdot\nabla\Phi_2\,dv$$

but

$$\iiint \nabla\phi_1 \cdot \nabla\phi_2 \, dv = \phi_2(p) \frac{\partial \phi_1(p)}{\partial n} \, ds \tag{75}$$

This implies the following

$$\iint \left[\iint H_1(p) F(p,q) H_2(q) \, ds(p) \right] ds(q)$$

$$= \iint \left[\iint H_2(p) F(p,q) H_1(q) \, ds(p) \right] ds(q)$$

$$= \iint \left[\iint H_1(p) F(q,p) H_2(q) \, ds(p) \right] ds(q) \tag{76}$$

Let

$$H_1 = \delta(a); \qquad H_2 = \delta(b)$$

where $\delta(a)$ is the delta dirac function at point a

$$\therefore F(a, b) = F(b, a).$$